A Journal of the Gesellschaft Deutscher Chemiker

Angewandte International Edition GDCh Chemie

www.angewandte.org

Accepted Article

Title: Self-Assembly of a Semiconductive and Photoactive Heterobimetallic Metal-Organic Capsule

Authors: Xiangquan Hu, Meirong Han, Li Shao, Chen Zhang, Le Zhang, Steven P Kelley, Chi Zhang, Jian Lin, Scott J Dalgarno, David A Atwood, Sisi Feng, and Jerry L. Atwood

To be cited as: *Angew. Chem. Int. Ed.* 10.1002/anie.202016077

Link to VoR: https://doi.org/10.1002/anie.202016077

WILEY-VCH

10.1002/anie.202016077

WILEY-VCH

COMMUNICATION

Self-Assembly of a Semiconductive and Photoactive Heterobimetallic Metal-Organic Capsule

Xiangquan Hu[a], Meirong Han[b], Li Shao[a], Chen Zhang[a], Le Zhang[c], Steven P. Kelley[a], Chi Zhang[d], Jian Lin[d], Scott J. Dalgarno[e], David A. Atwood[f], Sisi Feng*[b] and Jerry L. Atwood*[a]

Abstract: We report the synthesis of a novel metal-organic capsule constructed from six pyrogallol[4]arene macrocycles, which are switched together by 16 Fe(III) and 16 Co(II) ions. This supramolecular structure represents the first instance of a spheroidal heterometallic nanocage assembled through a one-step metal-ligand coordination approach. This new assembly also demonstrates an important proof of concept through the formation of multiple heterometallic metal-metal interactions within the capsule framework. Photophysical and electrochemical studies of self-assembled capsule films indicate their potential as semiconductors. These materials display unexpected photoelectric conversion properties, thus representing an emergent phenomenon in discrete metal-organic supramolecular assemblies.

The rational design and self-assembly of highly ordered, multi-component, spheroidal, supramolecular nanocages has been of great interest, as such species exhibit significant potential for application in areas such as host-guest recognition,[1-3] energy storage,[4,5] catalysis[6,7] and drug delivery.[8] However, compared to natural self-assembly, these functional entities often lack complexity or diversity, a feature that would be highly desirable for downstream application (and in some ways mimic biological systems).[9] For instance, self-assembled coordination nanocages are generally homometallic and are held together by only one type of noncovalent interaction. In contrast, large biological assemblies are often constructed from a diverse range of building blocks through multiple noncovalent interactions.[9b] There are limited reports detailing coordination nanocages assembled from more than one type of metal cation and interaction, but these resulted from dynamic covalent synthesis or stepwise assembly.[10,11] Heterometallic nanocages constructed directly from organic linkers and metal ions are at an embryonic stage and remain a significant synthetic challenge for the supramolecular chemist.

C-alkylpyrogallol[4]arenes (PgC*n*s, where "*n*" represents alkyl chain lengths) are bowl-shaped macrocyclic molecules and have been successfully used in the synthesis of mixed metal-organic nanocapsules (MONCs) through stepwise assembly.[12] These cyclic polyphenols, upon deprotonation, can be assembled with Ga^{3+} ions into a Ga-seamed hexameric cage structure comprising 12 metal ions ($Ga_{12}L_6$).[13] Incorporation of a secondary metal ion (Cu^{2+} or Zn^{2+}) into the pre-formed Ga-cages afforded capsules that are seamed together by 24 mixed Ga–Cu or Ga-Zn centers ($M_{24}L_6$).[14] Here we present the synthesis of a MONC assembled from PgC_5 subunits (Scheme 1) that is stitched together with Fe^{3+} and Co^{2+} ions and is of formula $[Fe_{16}Co_{16}(PgC_5)_6(Cl)_{16}(H_2O)_{32}]$ (**1**, Figure 1). It is important to note that the Fe^{3+}/Co^{2+}-seamed capsule is, to our knowledge, the only example of a spheroidal heterometallic nanocage assembled through a one-step metal-ligand coordination strategy.

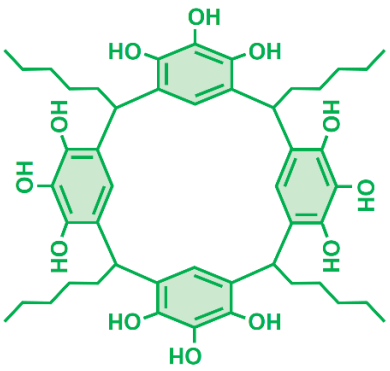

Scheme 1. Molecular structure of *C*-pentylpyrogallol[4]arene, PgC_5.

PgC_5 was prepared by using an acid catalyzed condensation reaction between pyrogallol and hexanal.[15] Compound **1** was synthesized by addition of $FeCl_3{\cdot}6H_2O$ and $CoCl_2{\cdot}6H_2O$ to a DMF solution containing PgC_5 and sodium methoxide, followed by sonication. Dark blue single crystals that were suitable for diffraction analysis (SCRD) formed upon standing over three days at room temperature, whilst bulk purity was confirmed by powder X-ray diffraction (PXRD, Figure S1).

SCRD found that capsules of **1** crystallize in an orthorhombic space group, with structure solution being carried out in the space group *Pcba*. The framework of **1** was found to contain 16 Fe^{3+} and 16 Co^{2+} ions, and 6 PgC_5 molecules (Figures 1 and S2), noting that this metal ratio is also supported by ICP-MS analysis. The metal-ligand arrangement of **1** is similar to that of the reported Fe^{2+}/Fe^{3+}-seamed hexameric capsule,[16] although the latter originated from a reaction of PgC*n* subunits with

[a] X. Hu, L. Shao, C. Zhang, S. P. Kelley, Prof. J. L. Atwood
Department of Chemistry, University of Missouri,
601 S. College Ave., Columbia, MO, 65211, USA
E-mail: atwoodj@missouri.edu
[b] M. Han, S. Feng,
Key Laboratory of Chemical Biology, Molecular Engineering of Ministry of Education, Institute of Molecular Science, Shanxi University, Taiyuan 030006, China
E-mail: ssfeng@sxu.edu.cn
[c] L. Zhang
Department of Chemistry, University of Texas, Austin, TX 78712, USA
[d] C. Zhang, L. Jian
Department of Mechanical and Aerospace Engineering, University of Missouri, Columbia MO 65211, USA
[e] S. J. Dalgarno
Institute of Chemical Sciences, Heriot-Watt University, Riccarton, Edinburgh EH14 4AS, United Kingdom
[f] D. A. Atwood
Department of Chemistry, University of Kentucky, Lexington, KY 40506, USA

Supporting information and the ORCID identification number(s) for the author(s) of this article can be found under:

https://doi.org/10.1002/anie.2018XXXXX

exclusively Fe^{3+} ions. That particular process is very slow, forming capsules over a period of 10 weeks with a yield ~2 % based on PgC*n*.

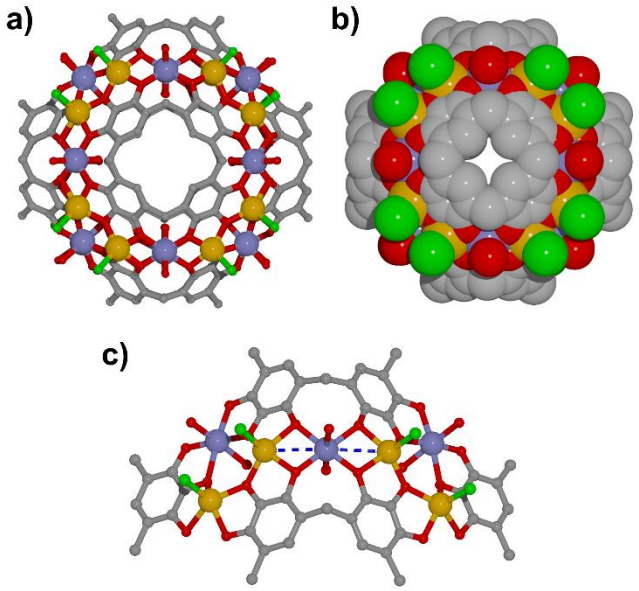

Figure 1. a) Ball and stick, and b) space-filling representations of **1**[25] showing 6 pyrogallol[4]arene units seamed together by 16 Fe^{3+} and 16 Co^{2+} ions. c) Side view of the capsule showing the coordination between metal ions and pyrogallol moieties including the [Fe_2CoO_3] array and bridging Co^{2+} ions. Fe-Co interactions are represented by blue dashed lines. Color codes: carbon (grey), oxygen (red), nitrogen (yellow), chloride (green), iron (orange), cobalt (blue), Hydrogen atoms and alkyl chains removed for clarity.

Inspection of the structure of **1** reveals that 16 Fe^{3+} metal centers are five-coordinate, have distorted square planar geometry, and are positioned out of the planes of the capsule walls (Figure S3). All the equatorial positions of these metal centers are occupied by upper-rim phenolato oxygens from PgC_5 moieties (64 Fe-O distances in the range of 1.92(3)-2.35(2) Å) and each axial position is occupied by a chloride ion (16 Fe-Cl distances in the range of 2.21(2)-2.25(2) Å). The 16 Co^{2+} metal centers adopt ideal octahedral geometries; each being coordinated to four equatorial phenolato oxygens and two axial aquo ligands. As shown in Figure 2c, the capsule framework is capped by eight [Fe_2CoO_3] triangular clusters, with 64 Co-O bond distances in the range of 2.00(2)-2.16(4) Å. The remaining 8 Co centers bridge neighboring [Fe_2CoO_3] units (Fe-Co-Fe angles: 170.48-173.97°), fully stitching the capsule seam together through metal-oxygen coordination bonds (32 Co-O distances in the range of 1.89(1)-2.10(3) Å). Metal complexes containing heterometallic metal-metal interactions are of great interest for the discovery of new types of interaction.[17] We found that there are 16 new types of heterometallic M-M interactions in the capsules (8 symmetry unique interactions). The distances between Fe and bridging Co ions ranging from 3.05(1) to 3.12(1) Å, which is close to the sum of covalent radii of 3.02 Å and much shorter than the sum of van der Waals radii of 3.84 Å.[18] This observation indicates the formation of metallophilic interactions.[17b] To the best of our knowledge, this is the first spheroidal coordination nanocage comprising heterometallic M-M interactions. In addition, the capsule is charge neutral, which is consistent with the deprotonation of 64 phenolic groups for charge balance (Figure S4). The remaining 8 PgC_5 upper-rim hydroxyl groups display hydrogen bonding interactions as evidenced by the short distances found between oxygen atoms (2.48(1)-2.66(1) Å). As expected, the IR spectra indicate that the intensity of the characteristic OH stretch of the Pg moieties is much weaker than the parent PgC_5 subunit (Figure S5).

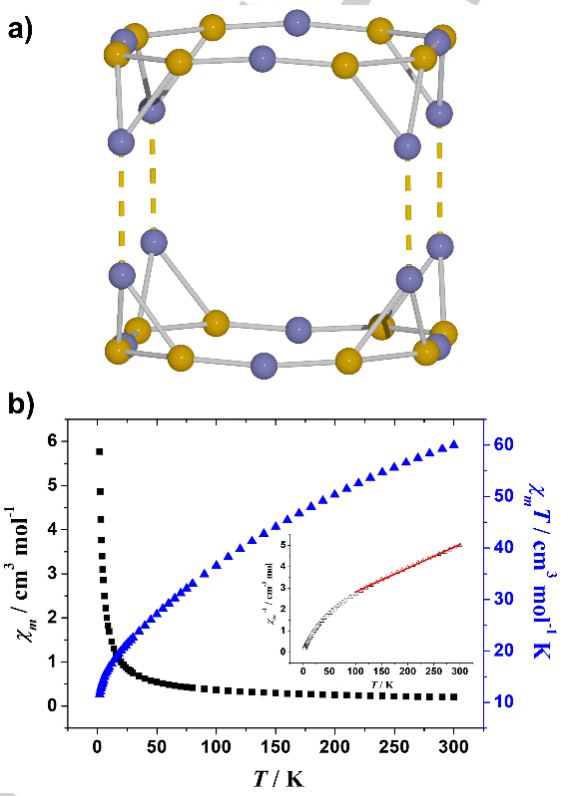

Figure 2. a) $Fe_{16}Co_{16}$ pseudo-cube found in **1** (metal-metal distances longer than 4 Å were represented by yellow dashed lines) and b) temperature dependence of χ_m, $\chi_m T$, and χ_m^{-1} (inset) collected in an applied field of 1000 Oe for **1**. Red solid line represents best fits.

Given that we have formed a new capsule comprising a $Fe_{16}Co_{16}$ pseudo-cube (edge ~1.1 nm, Figures 2a and S6), we reasoned that large magnetic coupling between the metal centers in the capsule seam may be possible. In addition to two crystallographically unique Co···Co distances of 4.90 Å and 4.94 Å, all metal-metal distances were found to be below 4 Å. This would therefore allow intramolecular magnetic exchange, which is rare in heterometallic nanocage systems[11a] The DC magnetic susceptibility data were recorded in the temperature range 2.0–300 K in an applied magnetic field of 1000 Oe. The χ_m, $\chi_m T$ vs. T plots for the capsule are shown in Figure 2b, where χ_m is the molar magnetic susceptibility. At 300 K, the $\chi_m T$ value of 60.0 cm^3 mol^{-1} K is lower than that expected for the sum of the Curie constants for sixteen non-interacting Co^{2+} (s = 3/2) and sixteen Fe^{3+} (s = 5/2) ions, with g = 2.00 (100.0 cm^3 mol^{-1} K). Upon lowering the temperature, $\chi_m T$ gradually decreases to a value of 11.5 cm^3 mol^{-1} K at 2.0 K, indicating the presence of antiferromagnetic (AF) exchange interactions. The large nuclearity of the cage and the number of unique exchange interactions prohibit any detailed quantitative analysis of the data; however, the molar magnetic susceptibility in the temperature range 100–300 K obeys the

Curie–Weiss law [χ_m = C/(T−θ)], i.e., C = 89.8 cm^3 mol^{-1} K and θ = −153.1 K (Figure 2b inset). The unusually large negative θ value confirms the existence of strong AF coupling among the metal centers. This may be caused by the effective overlap between the Fe and Co magnetic orbitals owing to their short distances associated with M-M interactions.[17a,19] Furthermore, the shape of the M/H plots is similar to that of an antiferromagnet, in which the M value increases rapidly at low fields, with no obvious saturation observed up to 70 kOe (Figure S7).

Due to their ease of fabrication, simple device structure and flexible design, molecule-based optic and electronic materials are of intense current interest and exhibit great potential in diverse applications including photoelectronic science, semiconductors and solar energy storage.[20,21] Amongst these functional species, metal complexes are very promising molecular building blocks due to their excellent photophysical and redox properties, despite being relatively scarce in applied literature.[17,20c] To our knowledge, no discrete coordination nanocages have been reported that have been shown to possess semiconducting and photoelectric conversion properties.

With this in mind, we fabricated self-assembled films of **1** using wet coating methods (see Supporting Information), with IR spectroscopy being used to confirm the identity of the crystals and films (Figure S8). Scanning electron microscopy (SEM) of films revealed a morphology with no clear evidence of high ordering (Figure S9), whilst PXRD studies show that capsule self-assembly in cast films lost most of the crystallinity compared to both single crystal and powder samples. However, the major peaks at low angle still indicate the existence of capsules (Figure S10). Unexpectedly, films of **1** generate photocurrents immediately and display good reproducibility under visible-light irradiation (λ > 420 nm) at a biased potential of 0.3 V vs. SCE (Figures 3a and S11). Such a phenomenon was not observed in PgC_5-based films (Figure S12). The anodic current suggests the typical feature of n-type semiconductors. To gain further insight into the electroactivity of the capsule films, Mott-Schottky (M-S) analysis were performed using electrochemical impedance techniques. The M–S plot was obtained at the frequency of 500 Hz in a 0.1 M sodium sulfate solution (Figure 3b). A flat band potential (E_{FB}) estimated from the extrapolation of the M–S plot is about −0.41 V *vs.* SCE (-0.17 vs. NHE). The positive slope further confirms the n-type semiconductor property of this material.[22] Since the flat band potential of an n-type semiconductor equals its Fermi level and the conduction band edge is more negative by about 0.10 V than the E_{FB}.[22b] Therefore, the conduction band potential (E_{CB}) of **1** is extrapolated to about −0.27 V vs. NHE. Combined with the bandgap energy calculated by the UV-vis diffuse reflectance spectra, the valence band potential (E_{VB}) of the capsules is calculated to be 2.21 V vs. NHE (Figure S13).

We propose that this unique charge transport phenomenon arise from the redox nature of the metal ions in **1**. It is known that metal-to-metal electron transfer between cobalt(II) and iron(III) centers in molecular systems can be induced by visible-light irradiation.[23] Thus, these redox-active metal centers on the capsule walls may act as electron carriers and the capsules could be either electron donor or acceptor. It appears that through-space charge transfer occurs between the neighboring capsules and this process may facilitate the separation and transfer of photogenerated electron–hole pairs.[22,24] This discovery signifies an important breakthrough in that it represents the first example of such discrete supramolecular nanocages. They have exciting potential applications in semiconductor and photoelectric materials, and this may, in turn, provide insight into charge transport in more complex biological systems such as bacterial photosynthesis.

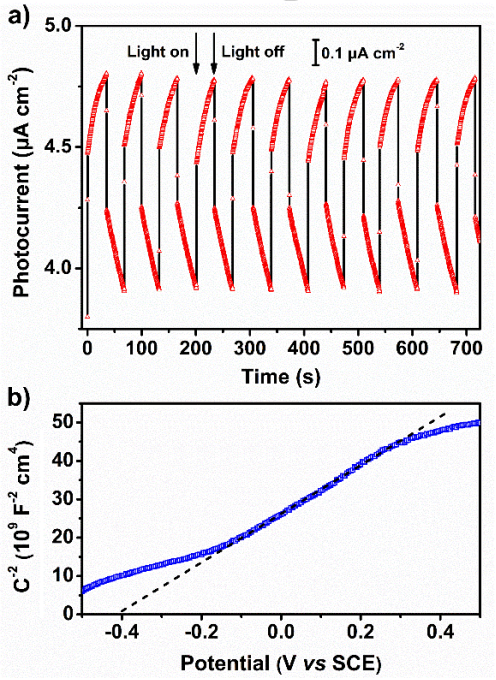

Figure 3. a) Photoelectric responses of self-assembled films of **1** under visible-light irradiation (λ > 420 nm). b) The Mott–Schottky (M–S) plot of the capsule films obtained at a frequency of 500 Hz in the dark.

In summary, we present the preparation of a $Fe^{3+}Co^{2+}$-seamed hexameric pyrogallol[4]arene nanocapsules comprising multiple heterometallic metal-metal interactions. This spheroidal cage-like nanoassembly exhibits rare intramolecular magnetic exchange within the heterometallic nanocage system, and large antiferromagnetic coupling was observed. Remarkably, the self-assembled capsule films show unexpected semiconducting and photoelectric conversion properties, a finding we are further exploring for other capsule structures. We expect that this work will open up new avenues for the synthesis of a more diverse library of coordination nanocages with innovative structures, metal ion composition and functionality. Examples of the latter may include potential utility in molecular nanomagnetism, molecule-based semiconductors and photoelectric devices.

Conflict of Interests

The authors declare no conflict of interest.

Keywords: Coordination cages • heterometallic metal-metal interactions • molecular magnetism • photoelectric conversion • molecule-based semiconductors

References

[1] a) I. V. Kolesnichenko. E. V. Anslyn, *Chem. Soc. Rev.* **2017**, 46, 2385-2390; b) T. R. Cook, Y. R. Zheng, P. J. Stang, *Chem. Rev.* **2013**, 113, 734-777.

[2] a) J. Zhou, G. Yu, F. Huang, *Chem. Soc. Rev.* **2017**, 46, 7021-7053; b) S. Chakraborty, G. R. Newkome, *Chem. Soc. Rev.* **2018**, 47, 3991-4016;

c) S. J. Dalgarno, S. A. Tucker, D. B. Bassil, J. L. Atwood, *Science* **2005**, 309, 2037-2039.

[3] a) T. D. Hamilton, G. S. Papaefstathiou, T. Friščić, D.-K. Bučar, L. R. MacGillivray, *J. Am. Chem. Soc.* **2008**, 130, 14366-14367; b) D. Zhang, T. K. Ronson, R. Lavendomme, J. R. Nitschke. *J. Am. Chem. Soc.* **2019**, 141, 18949-18953.

[4] a) Z. Niu, S. Fang, X. Liu, J.-G. Ma, S. Ma, P. Cheng, *J. Am. Chem. Soc.* **2015**, 137, 14873-14876; b) J. J. IV. Perry, J. A. Perman, M. J. Zaworotko. *Chem. Soc. Rev.* **2009**, 38, 1400-1417.

[5] Z. Niu, L. Wang, S. Fang, P. C. Lan, B. Aguila, J. Perman, J. Ma, P. Cheng, X. Li, S. Ma. *Chem. Sci.* **2019**, 10, 6661-6665.

[6] a) C. J. Brown, F. D. Toste, R. G. Bergman, K. N. Raymond, *Chem. Rev.* **2015**, *115*, 3012-3035; b) J. Kang, J. Rebek. *Nature* **1997**, 385, 50-52; c) M. Yoshizawa, J. K. Klosterman, M. Fujita. *Angew. Chem., Int. Ed.* **2009**, 48, 3418-3438.

[7] a) S. Gambaro, C. Talotta, P. D. Sala, A. Soriente, M. De Rosa, C. Gaeta, P. Neri. *J. Am. Chem. Soc.* **2020**, 142, 14914-14923; b) M. Yoshizawa, M. Tamura, M. Fujita, *Science* **2006**, 312, 251-254.

[8] a) D. Zhao, S. Tan, D. Yuan, W. Lu, Y. H. Rezenom, H. Jiang, L.-Q. Wang, H.-C. Zhou, *Adv. Mater.* **2011**, *23*, 90-93; b) T. R. Cook, V. Vajpayee, M. H. Lee, P. J. Stang, K.-W. Chi, *Acc. Chem. Res.* **2013**, *46*, 2464-2474.

[9] a) M. Schmittel, K. Mahata. *Angew. Chem., Int. Ed.* **2008**, 47, 5284-5286; b) D. B. Paul. *J. Hist. Biol.* **1988**, 21, 411-424.

[10] a) P. Jin, S. J. Dalgarno, J. L. Atwood, *Coord. Chem. Rev.* **2010**, 254, 1760-1768; b) F. J. Rizzuto, L. K. S. von Krbek, J. R. Nitschke, *Nat. Rev. Chem.* **2019**, 3, 204-222; c) M. Hardy, N. Struch, J. J. Holstein, G. Schnakenburg, N. Wagner, M. Engeser, J. Beck, G. H. Clever, A. Lützen, *Angew. Chem., Int. Ed.* **2020**, 59, 3195-3200.

[11] a) S. Sanz, H. M. O'Connor, E. M. Pineda, K. S. Pedersen, G. S. Nichol, O. MØnsted, H. Weihe, S. Piligkos, E. J. L. McInnes, P. J. Lusby, E. K.Brechin, *Angew. Chem., Int. Ed.* **2015**, 54, 6761-6764; b) Y.-Y. Zhang, W.-X. Gao, L. Lin, G.-X. Jin, *Coord. Chem. Rev.* **2017**, 344, 323-344.

[12] H. Kumari, C. A. Deakyne, J. L. Atwood. *Acc. Chem. Res.* **2014**, 47, 3080-3088.

[13] R. M. McKinlay, P. K. Thallapally, G. W. V. Cave, J. L. Atwood. *Angew. Chem., Int. Ed.* **2005**, 117, 5879-5882.

[14] H. Kumari, P. Jin, S. J. Teat, C. L. Barnes, S. J. Dalgarno, J. L. Atwood *Angew. Chem., Int. Ed.* **2014**, 126, 13304-13308.

[15] H. Kumari, L. Erra, A. C. Webb, P. Bhatt, C. L. Barnes, D. A. Deakyne, J. E. Adams, L. J. Barbour, J. L. Atwood. *J. Am. Chem. Soc.* **2013**, 135, 16963-16967.

[16] A. S. Rathnayake, H. W. L. Fraser, E. K. Brechin, S. J. Dalgarno, J. E. Baumeister, J. White, P. Rungthanaphatsophon, J. R. Walensky, S. P. Kelley, C. L. Barnes, J. L. Atwood. *J. Am. Chem. Soc.* **2018**, 140, 15611-15615.

[17] a) J. A. Chipman, J. F. Berry. *Chem. Rev.* **2020**, 120, 2409-2447; b) S. Schufort, P. Braunstein. *Chem. Soc. Rev.* **2011**, 40, 2741-2760.

[18] a) B. Cordero, V. Gómez, A. E. Platero-Prats, M. Revés, J. Echeverría, E. Cremades, F. Barragán, S. Alvarez. *Dalton. Trans.* **2008**, 2832-2838; b) S.-Z. Hu, Z.-H. Zhou, B. E. Robertson. *Z. Kristallogr.* **2009**, 224, 375-383.

[19] S. Feng, F. Jia, L. Lu, Z. Li, S. Zhang. *Chem. Commun.* **2016**, 52, 4294-4297.

[20] a) Y. Li. *Acc. Chem. Res.* **2012**, 45, 723-733; b) C. Wang, H. Dong, W. Hu, Y. Liu, D. Zhu. *Chem. Rev.* **2012**, 112, 2208-2267; c) Y.-G. Sun, S.-F. Ji, P. Huo, J.-X. Yin, Y.-D. Huang, Q.-Y. Zhu, J. Dai. *Inorg. Chem.* **2014**, 53, 3078-3087.

[21] K. M. Hutchins, T. P. Rupasinghe, L. R. Ditzler, D. C. Swenson, J. R. G. Sander, J. Baltrusitis, A. V. Tivanski, L. R. MagGillivray. *J. Am. Chem. Soc.* **2014**, 136, 6778-6781.

[22] a) Y. Bai, S. Zhang, S. Feng, M. Zhu, S. Ma. *Dalton Trans.* **2020**, 49, 10745-10754; b) S. Saha, G. Das, J. Thote, R. Banerjee. *J. Am. Chem. Soc.* **2014**, 136, 14845-14851.

[23] a) D. Aguilà, Y. Prado, E. S. Koumousi, C. Mathonière, R. Clérac. *Chem. Soc. Rev.* **2016**, 45, 203-224.

[24] J. Calbo, M. J. Golomb, A. Walsh. J. Mater. Chem. A. **2019**, 7, 16571-16597.

[25] CCDC 2047316 contains the supplementary crystallographic data for this paper. These data are provided free of charge by The Cambridge Crystallographic Data Centre.

10.1002/anie.202016077

WILEY-VCH

COMMUNICATION

Entry for the Table of Contents

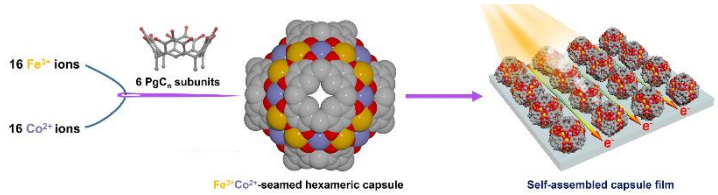

A mixed Fe^{3+}/Co^{2+}-seamed capsule comprising multiple heterometallic metal-metal interactions is presented here. This novel capsule displays unexpected semiconducting and photoelectric conversion properties.

Supporting Information

Table of Contents (12 pages)

Experimental details

Materials: Hexanal (W255718), hydrochloric acid (258148), sodium methoxide (164992), $CoCl_2 \cdot 6H_2O$ (255599) and $FeCl_3 \cdot 6H_2O$ (236489) were obtained from Sigma-Aldrich (St. Louis, MO). Pyrogallol (22779) was purchased from Chem-Impex International Inc. (Wooddale, IL). All solvents were purchased from Thermo Fisher Scientific and used without further purification.

Single crystal X-ray diffraction: the single crystal X-ray diffraction (XRD) data was collected on a Bruker Apex II CCD diffractometer at 100 (2) K using MoKα (1.5406Å) radiation with Inco-tech Microfocus tube. The high-resolution cutoff for diffraction from the best diffracting crystals was found to be around 1.30 Å, which is too low to resolve individual atoms and thus insufficient for most small molecule solution methods. However, likely because of both the presence of a large amount of unique, low-angle data due to the large unit cell and the fact that heavy atoms form an easily recognized, well-spaced sub-lattice, it was possible to locate the metal atom positions using an iterative dual space approach as implemented in SHELXT.[1] The normalized coordinates for an entire pyrogallol[4[arene moiety from another crystal structure were used to construct a rigid group that was fit to the metal sub-lattice in its expected position and refined.[2] From this point, it was possible to fit individual pyrogallol rings as rigid groups to peaks from the difference map until the entire unique half hexamer was built. Finally, axial ligands and some of the carbon atoms on the pentyl chains could be located from the difference map and were added to the model. The most important result from this model was that oxygen and chlorine atoms in axial positions could be distinguished from each other, likely because their separation from other atoms in the structure is greater than the resolution of the dataset. Chloride ligands were inevitably found axial to metal atoms with distorted square planar geometry in which the metal atom is positioned above the basal plane, while oxygen atoms were found in both exo- and endo-positions with respect to the capsule around metal atoms with ideal octahedral geometry. The model is insensitive to the assignment of metal atoms as Co or Fe, so all octahedral, oxo-ligated sites were assigned as Co, and all square pyramidal, Cl-ligated sites were assigned as Fe based on the greater stability of Fe(III) vs. Co(III). Figures were prepared using Diamond[3], X-seed[4] and Mercury[5] programs.

Powder X-ray Diffraction (PXRD): PXRD were measured on a Bruker X8 Prospector (Bruker AXS, Madison, WI, USA) single crystal diffractometer using Cu-Kα radiation from a microfocus source with multilayer optics (λ = 1.54060 Å, power = 45 kV, 0.60 mA). Samples were powdered by hand and loaded into 0.5 mm

diameter polyimide tubes. A series of 2-minute long photographs were taken while rotating the sample 360° about the phi axis. X-ray intensities were recorded across the 2θ range of 3° to 40° using an Apex II CCD area detector situated at a crystal-to-detector distance of 8.0 cm and with the detector remaining stationary throughout the measurement. Photographic data were reduced by radially integrating sectors of the photograph in shells of 0.02° in 2θ using the Bruker Apex3 software suite.[6] Powder XRD data was collected at ambient temperature using Cu (Kα) radiation Inco-tech Microfocus II (1.5406Å).

Elemental analyses (EA): EA were measured on a Vario EL III analyzer.

FTIR: IR spectra were recorded at room temperature using a Thermo Nicolet Avatar 360 FTIR Spectrometer in the 400–4000 cm^{-1} range.

Inductively coupled plasma mass spectrometry (ICP-MS): Samples were dissolved in Ultrapure 70% nitric acid. The resulting solutions were then diluted using 1% nitric acid and 18.2 MΩ water from Millipore Milli-Q® water purification system. ICP-MS data was collected on a NexION™ 350 ICP mass spectrometer. The individual results of the triplicate samples were averaged to determine the metal ratio.

Magnetism: DC magnetic susceptibility and magnetization measurements data were obtained with SQUID magnetometer (Quantum MPMS) in the temperature range 2.0-300K by using an applied filed of 1000 Oe. Diamagnetic corrections were applied to the data using Pascal's constants.

Photoelectric measurements: The photoelectric response experiments were performed on a RST5210F electrochemical workstation using a standard three-electrode configuration. The samples of PgC_5 and capsules (0.5 mg, respectively) were first dissolved in methanol (50 µl) and then coated onto FTO glasses (working electrodes, 1 cm^2 effective area). The solvents were removed by slow evaporation to yield the respective films. Platinum wire electrode was used as auxiliary electrodes. A saturated Hg/Hg_2Cl_2 (SCE) was used as the reference electrodes. A 500 W Xe lamp equipped with a 420 nm cut-off filter was employed as light source. The light source located 25 cm away from the surface of the FTO electrode. 0.1 M Na_2SO_4 aqueous solution was chosen as the supporting electrolyte. The Xe light equipped was turned on/off keeping 30 s and test for 30 s in the presence of the light source.

Mott-Schottky experiments: The Mott-Schottky plots of the capsule films were generated a RST5210F electrochemical workstation. The capacitance of the semiconductor-electrolyte interface was collected at 500 Hz, in the same electrolyte (0.1 M Na_2SO_4) and setup for photoelectric measurements.

UV-vis diffuse reflectance (DRS) spectroscopy: UV-vis DRS was performed by using a TU-1950 UV-vis spectrophotometer, during which $BaSO_4$ was adopted as the internal reflectivity standard.

Synthesis of PgC_5: Hexanal (10 mL, 0.08 mol) and pyrogallol (0.04 mol, 5.0 g) were mixed in 30 mL of ethanol and then 3.5 mL of concentrated HCl was added as a catalyst. The mixture was refluxed at 100 °C for 24 hours and cooled to room temperature. The resultant crystalline precipitate was filtered, washed with cold ethanol/water (1:1) and dried under vacuum. Yield is 35.5%.

Synthesis of 1: PgC_5, (0.1 mmol, 83.2 mg) and sodium methoxide (16 mg, 0.3 mmol) was dissolved 3 mL of N,N-dimethylformamide (DMF) and 6 mL of methanol (MeOH) in a 20 mL glass vial and was sonicated for 5 min at 45 °C. The resulting brown solution was cooled to room temperature. Thereafter, $FeCl_3{\cdot}6H_2O$ (72.2 mg, 0.267 mmol) and $CoCl_2{\cdot}6H_2O$ (63.5 mg, 0.267 mmol) were added. The mixture was further sonicated at 45 °C for 30 min to yield a dark blue solution. After placing at room temperature for three days, dark blue crystals were collected for single-crystal X-ray analysis. Thereafter, mother liquor was removed, and the crystals were washed with cold water/methanol (5:1) and dried in vacuum. Yield, 71 mg (47 %, with respect to PgC_5). Elemental analysis (EA): hypothesized $([Fe_{16}Co_{16}(PgC_5)_6(Cl)_{16}(H_2O)_{32}]{\cdot}12(DMF){\cdot}6(CH_3OH)$, ideal for $Fe_{16}Co_{16}C_{330}H_{492}O_{122}N_{12}Cl_{16}$ (%): C 44.14, H 5.48, N 1.87; Found: C 43.87, H 5.22, N 1.93. ICP-MS for $Fe_{16}Co_{16}$ complex: theoretical Fe/Co ratio=1.0; Fe/Co ratio based on ICP =1.0.

Crystallographic information for 1 (CCDC: 2047316)**:** dark blue plate, 0.22 x 0.18 x 0.02 mm^3, orthorhombic, space group P*bca* (No. 61), a = 38.580(8), b = 28.652(6), *c* = 38.794(8) Å, *V* = 42882(15) $Å^3$, *Z* = 4, D_c = 1.058 g cm^{-3}, F_{000} = 13904, Bruker APEX II CCD, MoKα radiation, λ = 0.71073 Å, *T* = 100 K, $2\theta_{max}$ = 34.6°, 159232 reflections collected, 13032 unique (R_{int} = 0.4188). Final *GOF* = 1.773, *R*1 = 0.2390, *wR*2 = 0.5274, *R* indices based on 5361 reflections with $I > 2\sigma(I)$ (refinement on F^2), 649 parameters, 57 restraints. Lp and absorption corrections applied, μ = 0.725 mm^{-1}.

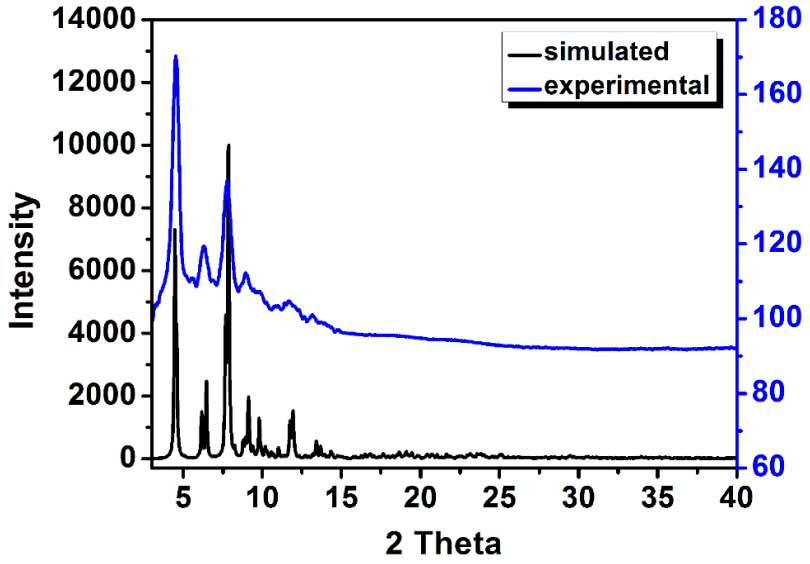

Figure S1. Simulated (blue line) and experimental (black line) powder X-ray Diffraction patterns of **1**.

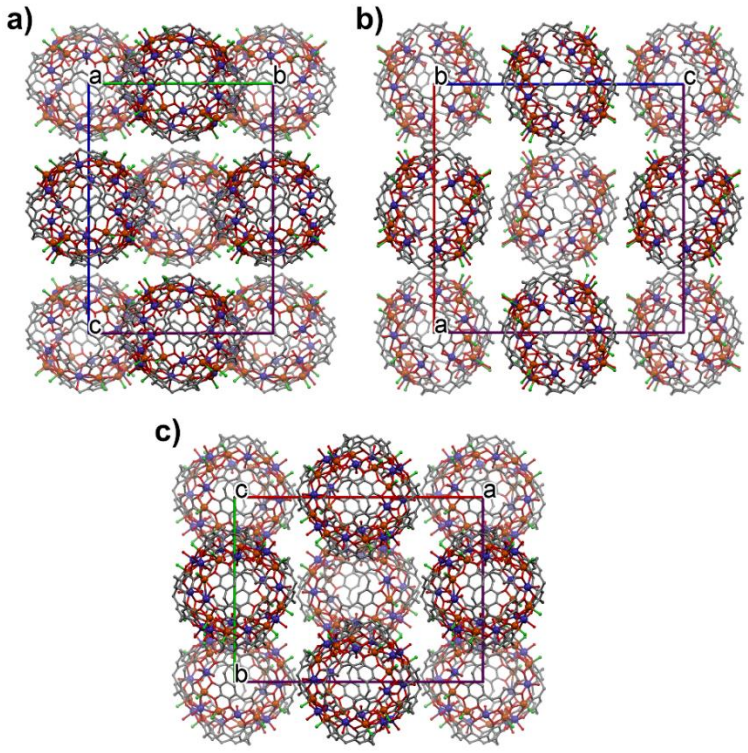

Figure S2. Extended view of **1** along [100] (a), [010] (b) and [001] (c) directions showing a close-packed array. Hydrogen atoms and alkyl chains are omitted for clarity. Color codes: grey (carbon), red (oxygen), green (chloride), orange (iron) and blue (cobalt).

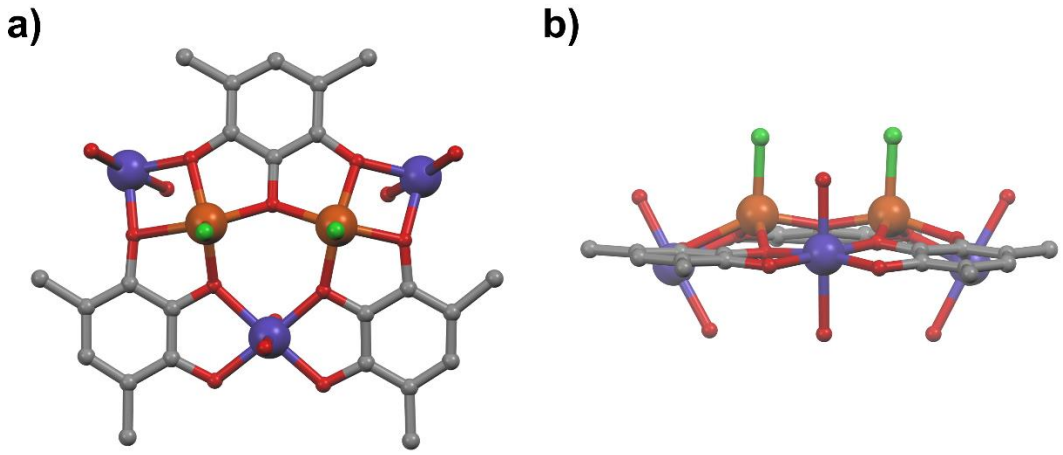

Figure S3. Arrangement of Fe^{3+} and Co^{2+} ions on the framework of **1**. Color codes: grey (carbon), red (oxygen), green (chloride), orange (iron) and blue (cobalt). Hydrogen atoms and alkyl chains have been omitted for clarity.

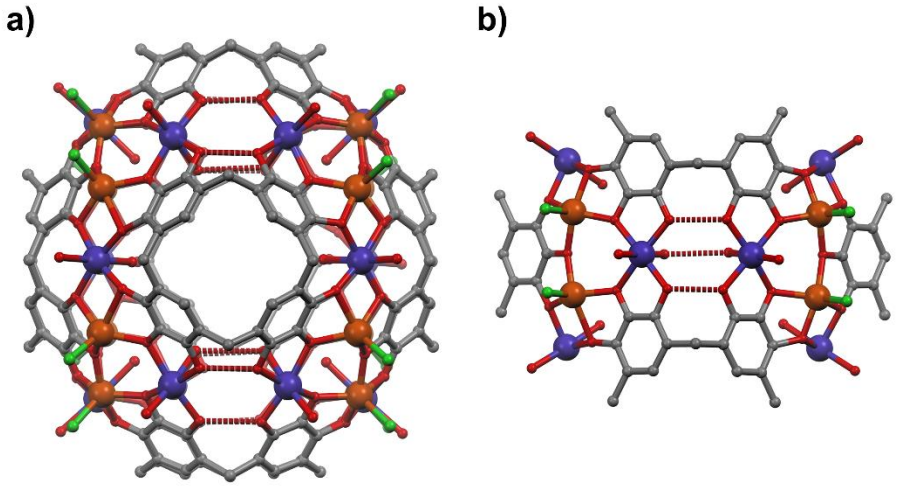

Figure S4. Stick representation of **1** showing the intramolecular hydrogen bonds Hydrogen bonds are represented by red dashed lines. Color codes: carbon (grey), oxygen (red), nitrogen (yellow), chloride (green), iron (orange), cobalt (blue). Hydrogen atoms and alkyl chains have been omitted for clarity.

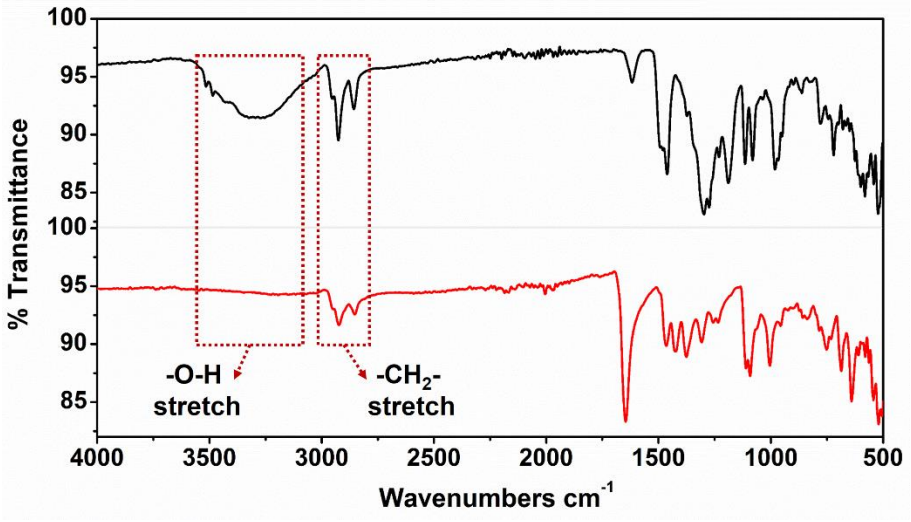

Figure S5. IR spectra of PgC_5 (black line) and **1** (red line). In the capsules, there is weakening of the hydroxyl vibration modes around 3250 cm^{-1}, and appearance of $-CH_2-$ stretching modes around 2900 cm^{-1}.

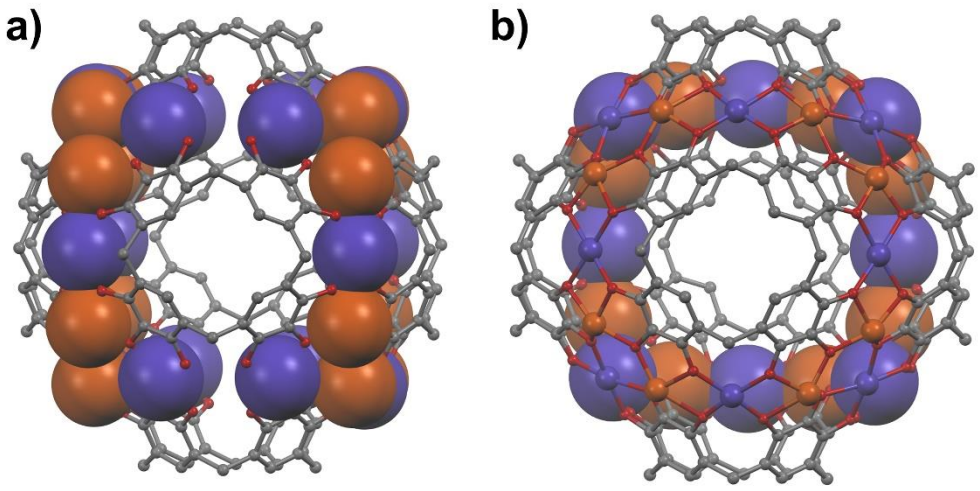

Figure S6. Side views of **1** showing a) $Fe_{16}Co_{16}$ pseudo-cube and b) Fe_8Co_8 pseudo-wheel. Metal centers were highlighted by space-filling model. The strong overlap of van der Walls spheres of Fe and bridging Co atoms clearly indicate the formation of heterometallic metal-metal interactions.[1,5] Color codes: carbon (grey), oxygen (red), nitrogen (yellow), chloride (green), iron (orange), cobalt (blue). Hydrogen atoms and alkyl chains have been omitted for clarity.

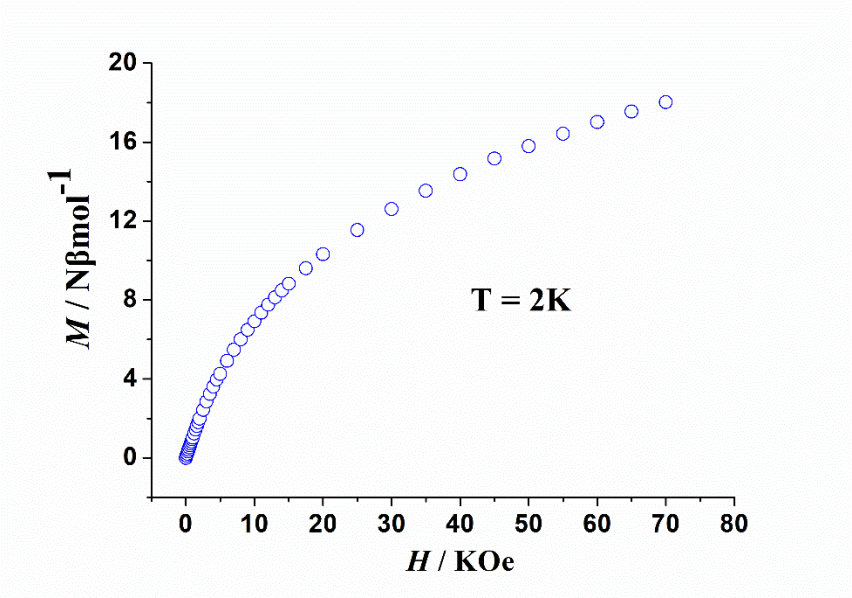

Figure S7. Magnetization (*M*) vs. field (*H*) for **1** in the indicated field.

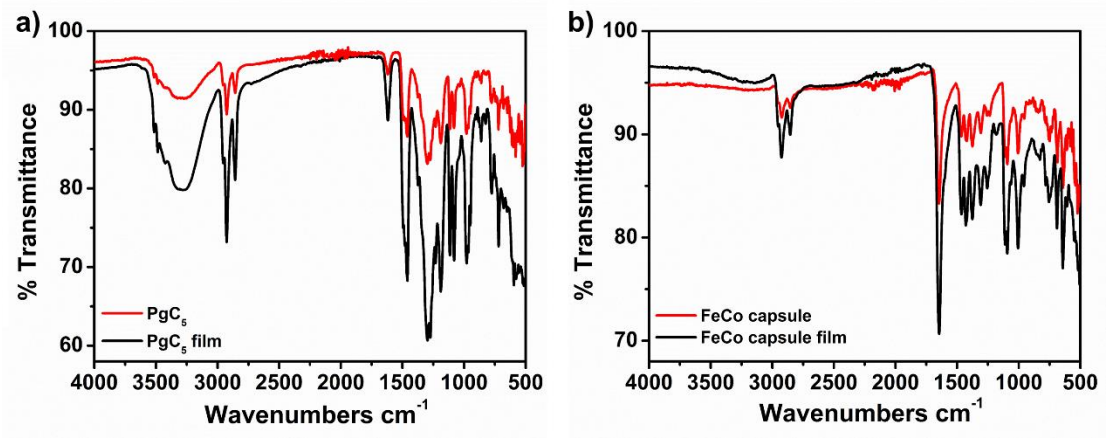

Figure S8. IR spectra of a) PgC_5 and PgC_5-based films; and b) self-assembled films of **1**.

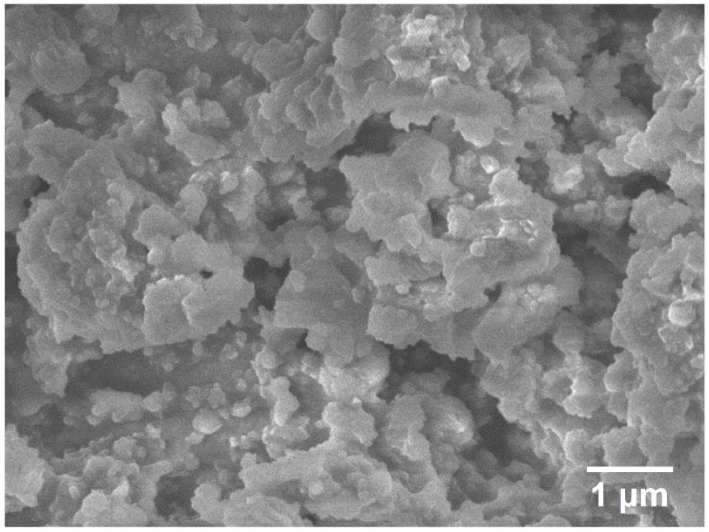

Figure S9. SEM image of self-assembled films of **1**.

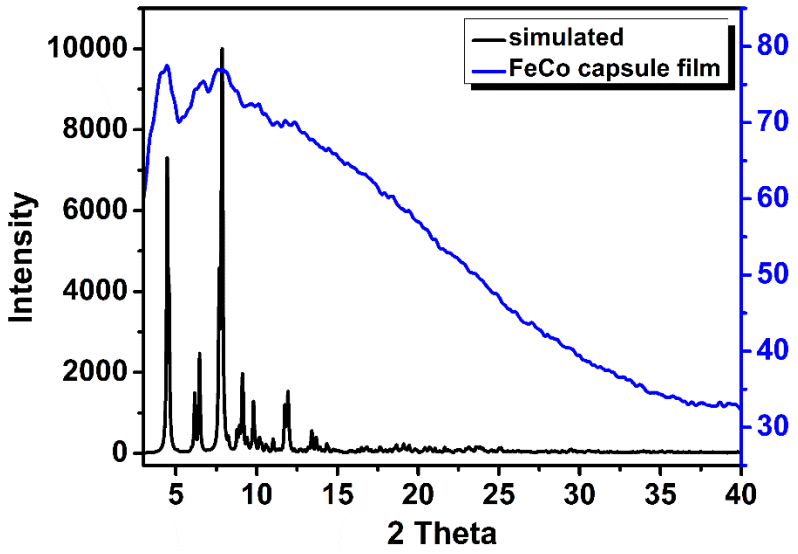

Figure S10. Powder X-ray diffraction of simulated single crystal structure (black line) and self-assembled films (blue line) of **1**. The capsule films lost most of the crystallinity compared to the single crystal structure. However, the major peaks at low angle still indicate the existence of capsules.

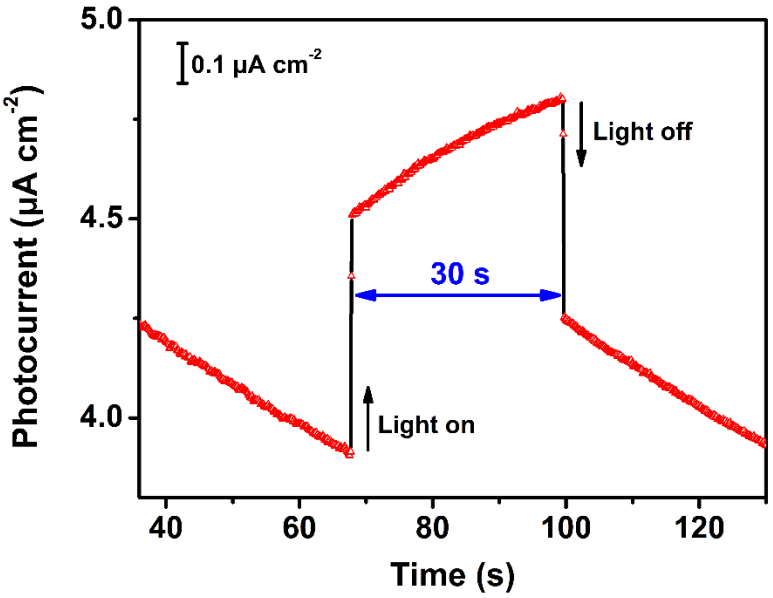

Figure S11. Photoelectric responses of self-assembled films of **1** induced by switching on and off the visible-light illumination (λ > 420 nm).

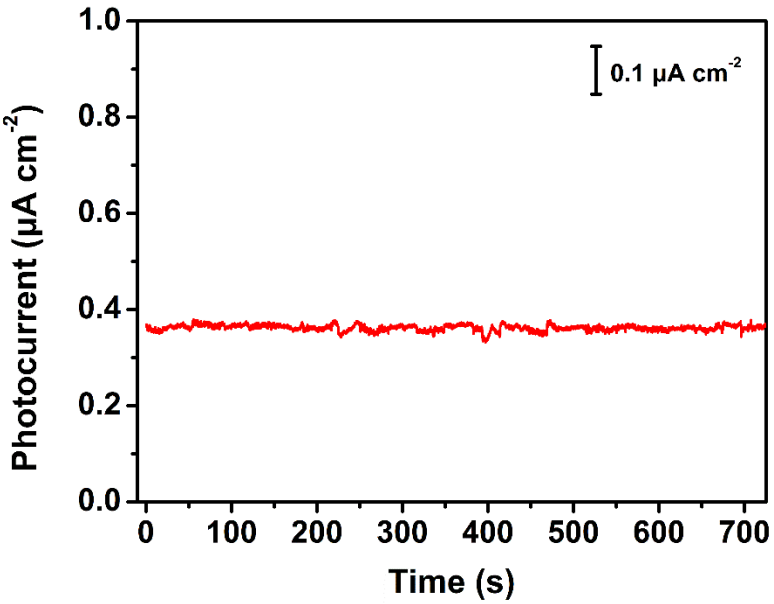

Figure S12. Photoelectric responses of PgC_5-based films (λ > 420 nm).

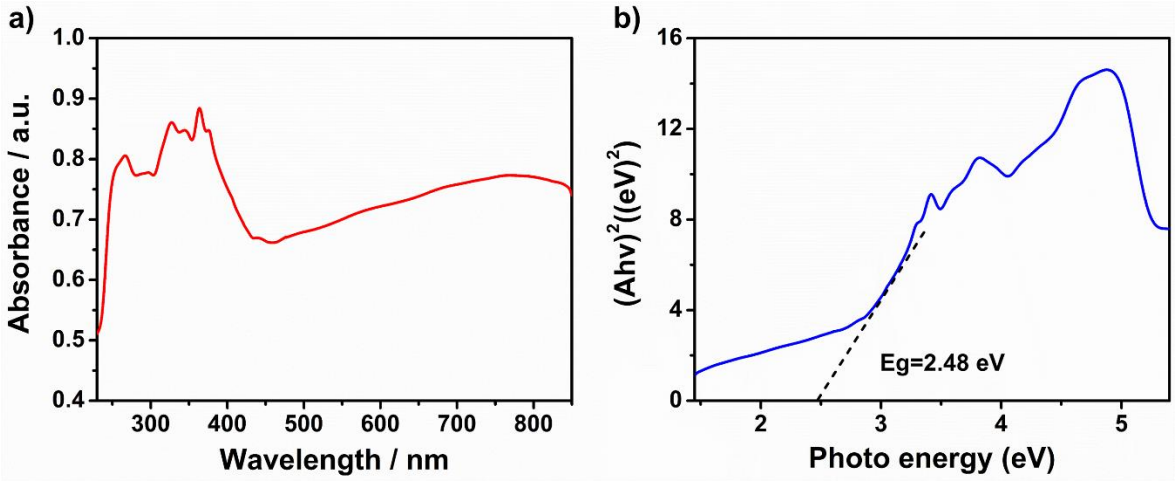

Figure S13. UV–vis DRS (a) and Tauc plot (b) of the self-assembled films of **1**, showing a band gab (Eg) of 2.48 eV.

References

[1] M. Sheldrick George, *Acta crystallographica. Section A, Foundations of crystallography.* **2008**, 64, 112-122.

[2] L. Shao, B. Hua, X. Hu, D. Stalla, S. P. Kelley, J. L. Atwood. *J. Am. Chem. Soc.* **2020**, 142, 7270–7275.

[3] W. T. Pennington. *J. Appl. Cryst.* **1999**, 32, 1028–1029.

[4] L. J. Barbour. *J. Supramol. Chem.* **2001**, 1, 189-191.

[5] C. F. Macrae, P. R. Edgington, P. McCabe, E. Pidcock, G. P. Shields, R. Taylor, M. Towler, J. van de Streek. *J. Appl. Cryst.* **2006**, 39, 453–457.

[6] Apex3, AXScale, and SAINT, version 2017.3-0, Bruker AXS, Inc., Madison, WI, **2017**.